Journal of Zhejiang University-SCIENCE B (Biomedicine & Biotechnology) in press
www.jzus.zju.edu.cn; www.springer.com/journal/11585
E-mail: jzus_b@zju.edu.cn

Research Article

https://doi.org/10.1631/jzus.B2500787

Dual-functional nanoplatform for simultaneous degradation of circRNA *CDR1as* and real-time monitoring of miR-7 in live cells

Yan HUANG[1], Jialin YE[1], Lan XU[1], Xingjie HU[2]✉, Nan CHEN[1]✉

[1]*College of Chemistry and Materials Science, The Education Ministry Key Lab of Resource Chemistry, Shanghai Engineering Research Center of Green Energy Chemical Engineering, and Shanghai Frontiers Science Center of Biomimetic Catalysis, Shanghai Normal University, Shanghai 200234, China*
[2]*School of Public Health, Shanghai Jiao Tong University School of Medicine, Shanghai 201318, China*

Abstract: Circular RNAs (circRNAs) are key post-transcriptional regulators with critical roles in pathogenesis, yet existing tools for their precise manipulation and functional analysis in living cells remain to be developed. A compelling therapeutic target in this field is the circRNA *cerebellar degeneration-related protein 1 antisense* (*CDR1as*), functioning as an oncogenic sponge for microRNA-7 (miR-7). Herein, we report a novel multifunctional The Zeolitic Imidazolate Framework-8 (ZIF-8)-based nanoplatform for the simultaneous disruption and real-time monitoring of the *CDR1as*/miR-7 regulatory axis. This system, named as DZ/MB@ZIF-8, co-encapsulates a designed set of DNAzymes for the catalytic cleavage of *CDR1as* as well as a molecular beacon (MB) for reporting on miR-7 activity. Following cellular uptake and lysosomal trafficking, the acidic microenvironment triggers nanoplatform disassembly, concurrently releasing the therapeutic and sensing components along with essential Zn^{2+} cofactors for DNAzyme activation. This system demonstrates efficient *CDR1as* degradation, which liberates miR-7 and inhibits the expression of its downstream oncogenic targets. Crucially, this therapeutic effect is directly correlated with a turn-on fluorescent signal from the MB, enabling the real-time, live-cell readout of circRNA regulation. This work establishes a versatile theranostic strategy that merges targeted gene regulation with intrinsic biosensing, offering a powerful platform for probing circRNA function and advancing RNA-based therapeutics.

Key words: Circular RNAs (circRNAs); The Zeolitic Imidazolate Framework-8 (ZIF-8); microRNA-7 (miR-7); DNAzyme; Gene regulation

1 Introduction

Circular RNAs (circRNAs) are a type of non-coding RNA with a covalently closed circular structure (Wu et al., 2024). They are structurally distinct from linear Messenger RNAs (mRNAs) and show higher stability in

✉ Nan CHEN, nchen@shnu.edu.cn
Xingjie HU, huxingjie@shsmu.edu.cn
Nan CHEN, https://orcid.org/0000-0001-8536-6631
Xingjie HU, https://orcid.org/0000-0002-0271-3843

Received Dec. 1, 2025; Revision accepted Apr. 8, 2026;
Crosschecked xxx. xx, 20xx; Published online xxx. xx, 20xx

cells (Jeck et al., 2013). In the past decade, circRNAs have become a research hotspot due to their important role in gene regulation (Jeck et al., 2013; Yang et al., 2017; Liu and Chen, 2022; Chen et al., 2025). Among them, *Cerebellar degeneration-related protein 1 antisense* (*CDR1as*), also known as *ciRS-7*, is one of the earliest discovered and most extensively studied of circRNAs (Meng et al., 2020). It contains more than 70 miR-7 binding sites and can act as a "molecular sponge" to adsorb miR-7, thereby regulating the expression of downstream target genes (Piwecka et al., 2017; Breuer et al., 2022; Shao et al., 2023). Studies have shown that *CDR1as* is abnormally expressed in various cancers (e.g., gastric cancer, breast cancer, glioma cells) and participates in the occurrence, development and metastasis of tumors through the miR-7-related pathways (Chen et al., 2019; Xu et al., 2025). Furthermore, the expression level of *CDR1as* is significantly correlated with the clinical stage and prognosis of cancer patients, demonstrating its potential both as a diagnostic marker and a therapeutic target for cancer (Shao et al., 2023; Xu et al., 2025).

By interfering with the expression of circRNAs, we can better understand their functions and assist in curbing the progression of diseases related to circRNAs, including cancer. Various circRNA manipulation technologies have emerged as tools for intervention in circRNAs (Yang et al., 2021; Liu et al., 2022; Wang et al., 2023; Zhang et al., 2023). For example, small interfering RNA (siRNA) or short hairpin RNA (shRNA) targeting the degradation of *CDR1as*, is applicable to pathological conditions (such as neuroinflammation) caused by its overexpression (Kihara et al., 2014; Zhang et al., 2022; Singh et al., 2024). Artificial circRNA or microRNA (miRNA) antagonists are designed to precisely regulate downstream pathways (Liu et al., 2021; Mao et al., 2021). More recently, clustered regularly interspaced short palindromic repeats-associated protein Cas (CRISPR-Cas) systems have been introduced to precisely edit *CDR1as* expression (Bloomer et al., 2022; Song et al., 2023). However, technical limitations hinder the further development and clinical application of these strategies, such as the cost and instability of synthetic RNA molecules, the low efficiency of intracellular delivery, and the complex protein components required in CRISPR-Cas systems (Behr et al., 2021). Thus, new, simple, efficient, and low-cost regulatory strategies for circRNAs need to be developed. As a catalytically active DNA molecule, DNAzyme has become an important tool for RNA research and application due to its high specificity and efficiency (Liu et al., 2024; Li et al., 2025): the high catalytic activity of DNAzyme makes it an ideal signal amplifier for RNA detection. Scholars have developed various DNAzyme-based circRNA detection methods, yet the direct utilization of DNAzyme for cleaving circRNA has rarely been reported (Mcconnell et al., 2021; Yu and Zhao, 2023; Feng et al., 2025). DNAzyme activation requires divalent metal ions such as magnesium, manganese and zinc. However, the endogenous metal ions concentrations are insufficient, which restricts its application in living cells (Victor et al., 2017; Fan et al., 2021). In addition, the intracellular delivery and release efficiency of DNAzyme need to be further improved for circRNA cleavage (Wang et al., 2019; Wu et al., 2021; Lee et al., 2023).

To evaluate the downregulation and therapeutic efficiency, it is necessary to extract RNA and analyze the expression levels of *CDR1as*, miR-7, and downstream genes by RT-qPCR (Li et al., 2023; Odame et al., 2023). This process is cumbersome and time-consuming, but more importantly, it is unable to assess the therapeutic

effect in real time and adjust accordingly. MiR-7 is the major effector of *CDR1as* in exerting its regulatory function, and the degradation of *CDR1as* will increase the intracellular abundance of miR-7 (Mehta et al., 2023; Fuchs wightman et al., 2024). Therefore, if the intracellular miR-7 levels can be characterized in real time and visually, it can indirectly reflect the cleavage efficiency and therapeutic effect of *CDR1as*.

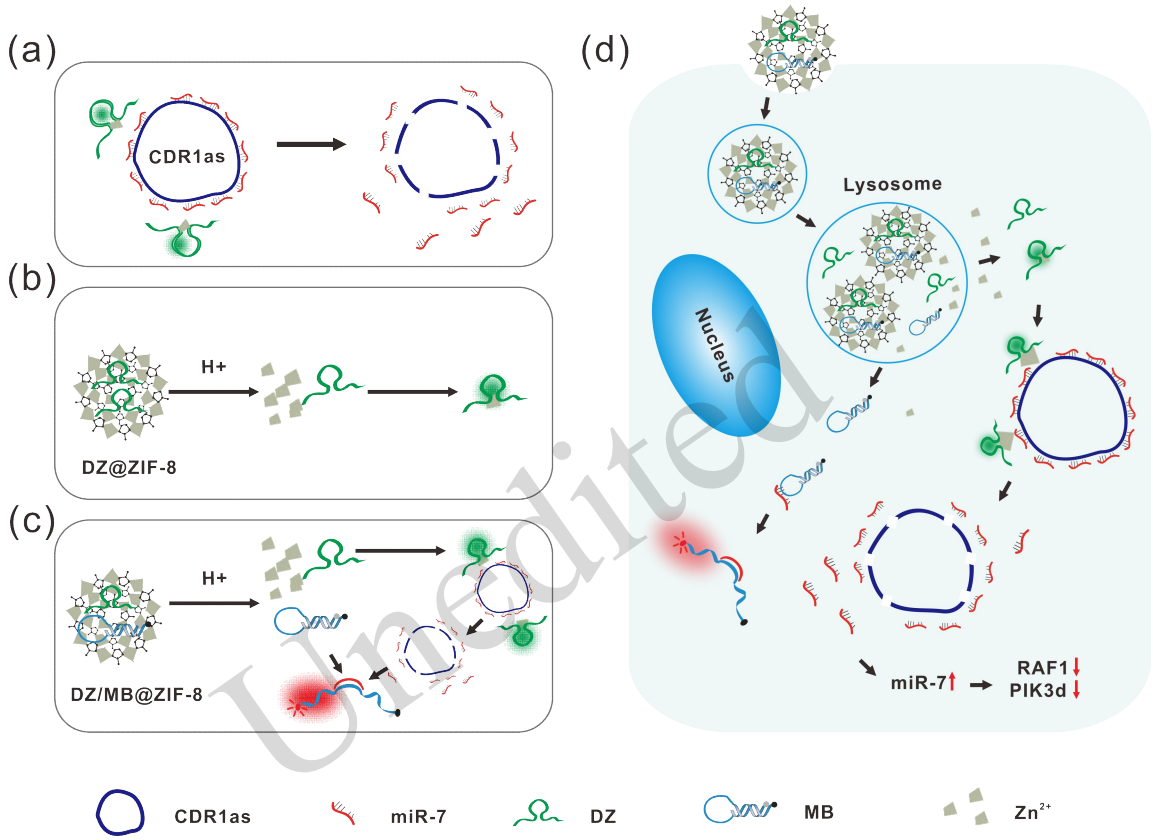

Fig. 1 Schematic illustration of the dual-functional DZ/MB@ZIF-8 nanoplatform for regulating and sensing the *CDR1as*/miR-7 axis. (a) DNAzymes are designed to recognize and cleave *CDR1as*. (b) The acidic environment triggers the disassembly of DZ@ZIF-8, resulting in the release of DZ and Zn^{2+} ions to form activated DZ. (c) The degradation of DZ/MB@ZIF-8 releases DZ, MB and Zn^{2+} cofactors, leading to DZ activation and *CDR1as* cleavage. The binding of the freed miR-7 to the MB generates a fluorescent signal. (d) Following cellular uptake and lysosomal trafficking, DZ/MB@ZIF-8 is disassembled. The released Zn^{2+} activates DZ, which then cleaves *CDR1as*. This frees miR-7, which can in turn inhibit the expression of its downstream target genes (e.g., *RAF1*, *PIK3CD*). The simultaneous binding of the freed miR-7 to the MB generates a fluorescent signal, providing a real-time readout of the platform's therapeutic activity. Abbreviations: ZIF-8, Zeolitic Imidazolate Framework-8; MB, molecular beacon; DZ, DNAzyme; miR-7, microRNA-7; *CDR1as*, *Cerebellar degeneration-related protein 1 antisense*; *RAF1*, *Raf-1 proto-oncogene, serine/threonine kinase*; *PIK3CD*, *phosphatidylinositol-4,5-bisphosphate 3-kinase catalytic subunit delta*.

The Zeolitic Imidazolate Framework-8 (ZIF-8) has emerged as a promising nanocarrier for DNAzymes due to its unique properties (Troyano et al., 2019; Zhao et al., 2023; Zeng et al., 2024). Studies have shown that ZIF-8 can encapsulate various biomolecules, maintain their activity and ensure biocompatibility in physiological conditions (Zhang et al., 2021; Wei et al., 2023; Gao et al., 2025). ZIF-8 is known to degrade

under acidic conditions, which are typically found in intracellular compartments such as endosomes and lysosomes (Mishra et al., 2023). This degradation releases the encapsulated DNAzymes in a controlled manner, ensuring that they reach their target site in an active form. Moreover, ZIF-8 serves as an intrinsic Zn^{2+} source, which is essential for the catalytic activity of DNAzymes (Wu, et al., 2021; Ye et al., 2021). This dual role of ZIF-8 as both a carrier and a cofactor source is particularly advantageous in Zn^{2+}-dependent DNAzyme-based therapeutic applications.

In this study, we designed a ZIF-8-based nanoplatform co-encapsulating *CDR1as*-targeting DNAzymes and a miR-7-targeting molecular beacon. After endocytosis, DZ/MB@ZIF-8 is encapsulated into lysosomes and disintegrated. With the help of Zn^{2+}, activated DNAzymes can effectively cleave *CDR1as*. Real-time visualization of intracellular miR-7 is achieved via the fluorescence of a MB probe. Furthermore, the regulatory effects of *CDR1as*/miR-7/mRNA axis are confirmed by subsequent inhibition of downstream genes regulated by miR-7, including *RAF1* (*Raf-1 proto-oncogene, serine/threonine kinase*) and *PIK3CD* (*phosphatidylinositol-4,5-bisphosphate 3-kinase catalytic subunit delta*). This dual functional DZ/MB@ZIF-8 nanoplatform achieves simultaneous circRNA regulation and real-time monitor in living cells, providing a novel approach to exploring the biological process and therapeutic regulation of circRNAs (Fig. 1).

2 Results and discussion

2.1 Design and in vitro validation of *CDR1as*-targeting DNAzyme set

CDR1as has a unique reverse splicing structure that distinguishes it from its cognate linear CDR1 mRNA. DNAzymes are capable of specifically recognizing the back-splice junction (BSJ) sequence of *CDR1as*, avoiding interference from homologous linear RNAs. We chose 8-17 DNAzyme and 10-23 DNAzyme, two DNAzymes that have been widely used in mRNA regulation, and tested their ability to cleave *CDR1as*. 8-17 DNAzyme is a type of Zn^{2+}-dependent DNAzyme that cleaves the rA-rG base junctions of RNA substrates (W et al., 1997; Cepeda-Plaza and Peracchi, 2020), while 10-23 DNAzyme is a type of Mg^{2+}-dependent DNAzyme that cleaves the rR-rY (where R is A or G, and Y is U or C) base junctions of RNA substrates (W et al., 1997; Schubert, 2003). DNAzymes consist of a two-sided binding arm for substrate RNA recognition and a middle sequence that form the cleavage center upon the binding and activation of metal ions. The back-splice junction (BSJ) sequence is essential for circular *CDR1as* formation, hence DNAzyme (DZ1) targeting that region was designed. To ensure and enhance the cleavage efficiency on *CDR1as*, additional DZ targeting sequences outside of BSJ were introduced. We designed both a DZ2 targeting sequence close to BJS and a DZ3 targeting sequence far from BJS (Figs. 2a-2b, S1a and Table S1).

Based on the cleavage principle of DNAzyme, its secondary structure must align with the corresponding catalytic domain (Nurmi et al., 2024). We used the RNAstructure software to predict the secondary structure formed by the binding of the three DZ to the substrate RNA (Zuker, 2003; Agarwal et al., 2015; Sato et al., 2021). All three 8-17 DZs successfully attached to the targeted sequence substrates and formed specific secondary

structures of catalytic domains (Fig. 2c). To investigate the interaction and cleavage effects of the designed DZs, three RNA sequences derived from the *CDR1as* and the three DZ sites therein were concatenated to form a 783-nucleotide-long RNA, *S-CDR1as*, serving as an in vitro RNA mimic of *CDR1as* (Fig. S1c and Table 2). Three 8-17 DZs, either individually or as a combination, were separately incubated with the substrate in the presence of Zn^{2+}, and their nucleic acid cleavage efficiency was examined and compared using gel electrophoresis. Upon treatment by DZs, the intensity of the bands of *CDR1as* were reduced and short RNA fragments were observed, indicating RNA recognition and cleavage by the designed 8-17 DZs (Figs. 2d and 2e). Quantitative analysis pointed to DZ2 as the most powerful single DZ for *CDR1as* cleavage. This superior efficiency can be attributed to its favorable structural context. The target site of DZ2 is located near the 5' region of the circRNA, which possesses relatively low secondary structure complexity. In contrast, DZ1 targets the highly constrained backsplice junction (BSJ), and DZ3 is situated in a region densely populated with miR-7 binding sites that likely create steric hindrance due to interactions with RNA-binding proteins (Hansen et al., 2013; Ashwal-Fluss et al., 2014; Shafaghat et al., 2025). Furthermore, the combined DNAzyme set of DZ1+2 is more efficient than the BSJ-targeting DZ1 alone, demonstrating a synergistic effect (Figs. 2d and 2e). This is likely due to the spatial proximity of site 1 and site 2 within the three-dimensional structure of *CDR1as*, allowing for a 'cooperative cleavage' effect where initial cleavage by DZ1 alters local RNA folding, rendering site 2 more accessible for DZ2.

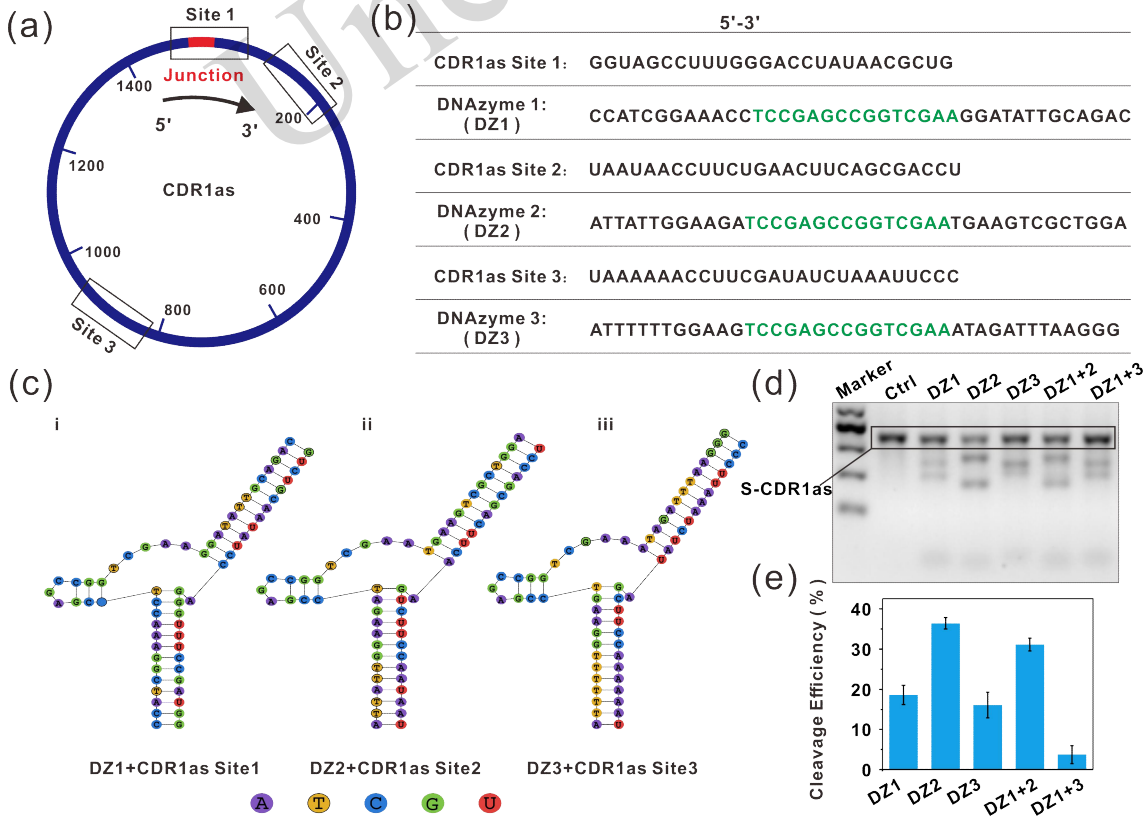

Fig. 2 Design and cleavage activity of DNAzymes targeting *CDR1as*. (a) Schematic representation of *CDR1as* and the three cleavage sites (site1, site2 and site3) recognized by 8-17 DNAzyme. (b) Sequences of the three cleavage sites. The catalytic

core of the DNAzyme is shown in green. (c) Predicted secondary structures of the DZ-target complexes using RNAstructure software. (d) Gel electrophoresis analysis of the cleavage of DZ and S-*CDR1as*. (e) Cleavage efficiency of individual or combined DZ quantified using Image J software. The data are expressed as mean ± SD(*n*=3). Abbreviations: DZ, DNAzyme; *CDR1as*, Cerebellar degeneration-related protein 1 antisense; S-*CDR1as*, substrate RNA derived from *CDR1as* containing three DZ-argeted sequences.

Similarly, three 10-23 DNAzymes targeting the *CDR1as* sequence—at BSJ (DZ1), close (DZ2) or far (DZ3) from BJS—were designed and synthesized (Figs. S2a and S2c). Individual DZs or DZ combinations were incubated with the *CDR1as* mimic RNA in the presence of Mg^{2+}, and their nucleic acid cleavage efficiency was determined by gel electrophoresis. The gel and quantitative analysis results were highly consistent with those obtained with 8-17 DNAzyme. Combined DNAzyme sets of DZ1+2 showed more efficient cleavage than other DZ combinations. (Figs. S2d and S2e). These results demonstrated that both 8-17 DNAzyme and 10-23 DNAzyme could cleave *CDR1as* in vitro, and DZs targeting different part of *CDR1as* exhibited differences in activity. Thus, combining the BSJ-targeting DZ1 with a DZ that recognize the sequence in proximity may significantly enhance the ability to degrade and inhibit *CDR1as*.

2.2 DNAzyme set regulates the *CDR1as*/miR-7/ *RAF1* and *PIK3CD* axis

Having confirmed the effectiveness the designed DNAzyme to cleave *CDR1as* in vitro, the functionality of DNAzyme in live cells was assessed. We hypothesized that DZ could cleave *CDR1as* and disrupt the miR-7 adsorption sponge. The results showed that increased intracellular miR-7 inhibited expression of downstream genes (Fig. 3a). Individual DNAzyme or their combinations were transfected into MCF-7 cells via a transfection reagent. After 48 hours of co-incubation in the presence of 0.5 mmol/L Zn^{2+}, the RNA levels of *CDR1as* were assessed by RT-qPCR. All DZ-treated cells showed significant decrease in *CDR1as* levels, and the combination of DZ1+2 appeared to be the most effective inhibitor of *CDR1as* (Fig. 3b). This result validated that DNAzyme could serve as a potent tool for cleaving and regulating intracellular circRNAs. Next, we investigated whether the cleavage of *CDR1as* can regulate its downstream gene pathways. Research in osteosarcoma cells has shown that *CDR1as* regulates the expression of cancer-related genes such as *PIK3CD* and *RAF1* through miR-7 (Xu et al., 2018). We also identified the miR-7-pairing sequence in the coding region of *RAF1* mRNA and *PIK3CD* mRNA using TargetScan software (Shafaghat, et al., 2025), suggesting these genes are directly regulated by miR-7 (Fig. S3). To investigate their responsiveness to miR-7 in MCF-7 cells, exogenously synthesized miR-7 was overexpressed (OE-miR-7) in MCF-7 cells and the expression levels of *RAF1* and *PIK3CD* were determined. A significant downregulation of both *RAF1* and *PIK3CD* was observed, confirming them as downstream genes regulated by the *CDR1as*/miR-7 axis (Fig. 3c). We then transfected the cells with the optimal combination of DZ1+2 (indicated as DZ) and observed decreased mRNA levels of *RAF1* and *PIK3CD* (Fig. 3d). The above results proved that the DZ delivered via a standard transfection reagent could effectively knock down *CDR1as* in MCF-7 cells and thereby cause a decrease in *RAF1* and *PIK3CD* mRNA levels, validating the proposed pathway.

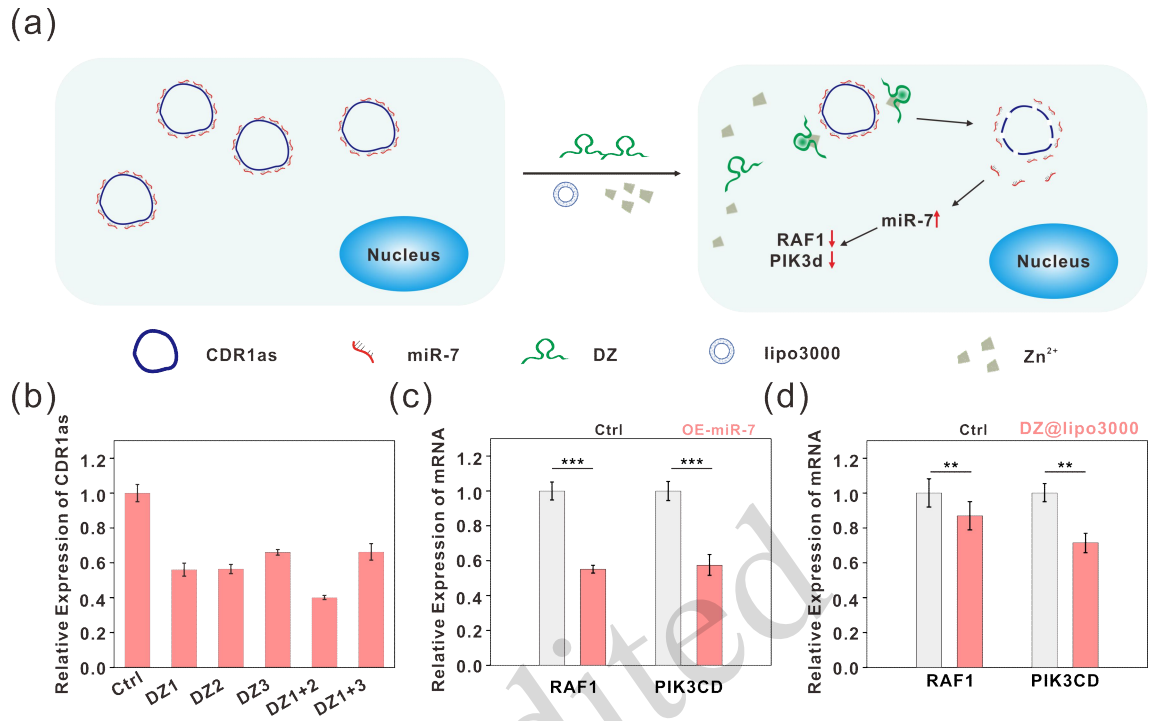

Fig. 3 DZ regulates the *CDR1as*/miR-7/ *RAF1* and *PIK3CD* axis. (a) Schematic diagram showing the DZ-mediated regulation of *CDR1as* and downstream gene network. (b) Expression levels of *CDR1as* upon indicating DZ treatment as quantified by RT-qPCR. (c) mRNA levels of *RAF1* and *PIK3CD* upon miR-7 overexpression as quantified by RT-qPCR. (d) mRNA levels of *RAF1* and *PIK3CD* under DZ(DZ1+2) treatment as quantified by RT-qPCR. Data are expressed as mean ± SD (n=3), *p < 0.05, **p < 0.01, ***p < 0.001 compared with the control group. Abbreviations: DZ, DNAzyme; miR-7, microRNA-7; *CDR1as*, *Cerebellar degeneration-related protein 1 antisense*; lipo3000, Lipofectamine 3000; OE-miR-7, overexpressed miR-7; *RAF1*, *Raf-1 proto-oncogene, serine/threonine kinase*; *PIK3CD*, *phosphatidylinositol-4,5-bisphosphate 3-kinase catalytic subunit delta*.

2.3 Synthesis and characterization of the DZ@ZIF-8 nanocomplex

Next, we designed and constructed a nanocomplex to deliver DZ into mammalian cells. ZIF-8 is a type of zinc-based MOF material with mild synthesis conditions, suitable for carrier and intracellular delivery of biomolecules such as proteins and nucleic acids. ZIF-8 can disintegrate in the acidic environment of lysosomes and release bioactive cargos. In particular, the released zinc ions can serve as essential co-factors to activate 8-17 DNAzymes. Therefore, ZIF-8 was chosen as the nanocarrier for DZ intracellular delivery in the next step (Fig. 4a). ZIF-8 nanoparticles were synthesized by rapid colloidal chemistry at room temperature, then DNAzymes were loaded onto the surface of ZIF-8 by electrostatic adsorption, forming DZ@ZIF-8 nano-complexes. Scanning Electron Microscopy (SEM) analysis revealed that the synthesized ZIF-8 nanoparticles exhibited a hexagonal shape, with an average size of 92.8±3.50 nm (Figs. S4a and S4b). After the adsorption of DNAzyme on the ZIF-8 surface, the original polygonal angles became smoother and the particle size increased to 96.6±4.58 nm (Figs. 4b and 4c). The hydration radius was determined using DLS: it increased

from 122.4 nm of ZIF-8 to 164.2 nm of DZ@ZIF-8 (Fig. S4c). Zeta potential analysis showed that the surface

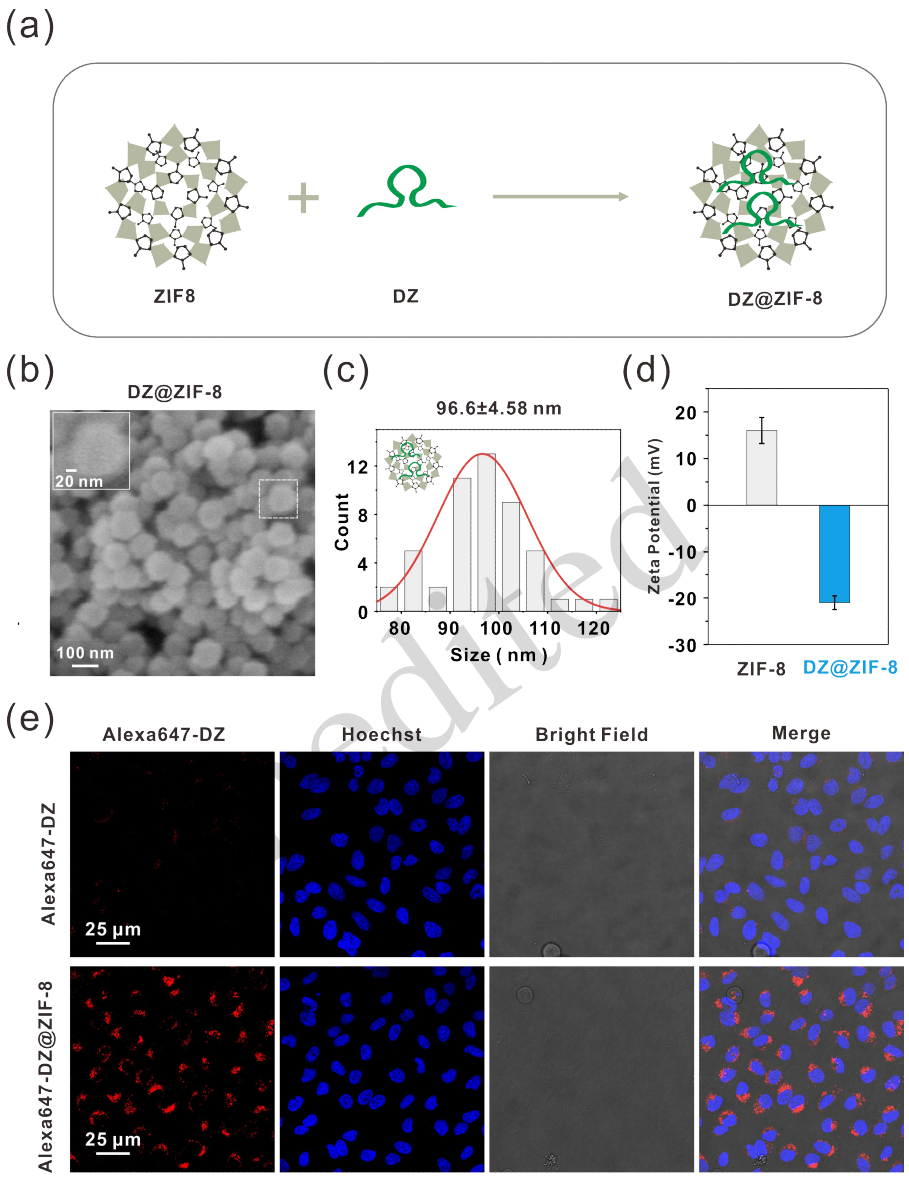

Fig. 4 Synthesis and characterization of DZ@ZIF-8 nanocomplex. (a) Schematic of the DZ-loaded ZIF-8 nanoparticle (DZ@ZIF-8). (b, c) SEM images and corresponding particle size distribution analysis of DZ@ZIF-8. The inset in (b) is a magnified view of the area indicated by the white dashed box. Scale bar in inset = 20 nm (d) Zeta potentials of ZIF-8 and DZ@ZIF-8. (e) Cells were incubated with Alexa647-DZ or Alexa647-DZ@ZIF-8 for 24 h and imaged by confocal microscopy (Alexa647: red; Hoechst: blue; Scale bar=25 μm). The data are expressed as mean ± SD(n=3). Abbreviations: ZIF-8, Zeolitic Imidazolate Framework-8; DZ, DNAzyme; SEM, scanning electron microscope.

charge changed from +15 mV of ZIF-8 to -21 mV of DZ@ZIF-8 (Fig. 4d). The loading of DZ on ZIF-8 was examined by differential subtraction fluorescence and the loading efficiency was up to 55.54 μg/mg (Figs. S4d and S4e). The biocompatibility of DZ@ZIF-8 was determined by MTT assays, and its toxicity at the concentration of 30 μg/mL and below was negligible (Fig. S4f). To ensure its suitability for biological

applications, the colloidal and structural stability of the nanoplatform was evaluated. DZ@ZIF-8 nanoparticles were incubated in DMEM supplemented for 7 days. The hydrodynamic size and polydispersity index (PDI) remained relatively constant (Fig. S5a), indicating excellent colloidal stability. Furthermore, no significant fluorescence from Cy3-labeled cargo was detected in the supernatant over a 24-h period (Fig. S5b), confirming that the DNA probes had stably encapsulated within the ZIF-8 framework without premature leakage in physiological media. To inspect the intracellular delivery of DZ by ZIF-8, DNAzyme labelled with Alexa647 was utilized to construct DZ@ZIF-8 exhibiting fluorescence. Both Alexa647-DZ@ZIF-8 and free Alexa647-DZ were incubated with MCF-7 cells for 24 h, and the intracellular fluorescence was examined using a confocal microscope. Obvious fluorescence was detected in cells treated with Alexa647-DZ@ZIF-8, while no fluorescence was detected in cells incubated with free Alexa647-DZ (Fig. 4e). This result validated ZIF-8 as effective nanocarriers for the intracellular delivery of nucleic acid.

The key step for DZ@ZIF-8 to exert its expected function within cells is the disintegration within acidic lysosomes (Fig. 5a). The responsiveness of DZ@ZIF-8 to acidic pH conditions was investigated by incubating it in solutions with either pH 7.4 or pH 5.5 for 2 hours. The mixture was then centrifuged and the supernatant was analyzed by gel electrophoresis. A DZ band appeared in the supernatant of the sample at pH 5.5, while no such band was detected in the supernatant of the sample at pH 7.4, indicating that the degradation of DZ@ZIF-8 only occurred at pH 5.5 (Fig. S5c). Importantly, the fluorescence properties of Cy3-DZ remained unchanged across different pH buffers (Fig. S5d), confirming that the degradation of the material in an acidic lysosomal environment does not affect the fluorescence of Cy3 and ensuring the accuracy of subsequent intracellular detection of miRNA-7. Furthermore, supernatants of different pH were applied to S-*CDR1as* to compare their enzymatic activity in vitro. Similarly, only the supernatant of the sample at pH 5.5 could cleave S-*CDR1as* (Fig. 5b), validating the functionality of DNAzymes and Zn^{2+} released from DZ@ZIF-8.

Subsequently, the intracellular disintegration of DZ@ZIF-8 was investigated. Alexa647-DZ@ZIF-8 was incubated with MCF-7 cells for 16 h before observation using a confocal microscope, and obvious intracellular fluorescence was detected. Importantly, the fluorescence of Alexa647-DZ showed significant co-localization with stained lysosomes, implying that DZ@ZIF-8 accumulated in lysosomes following endocytosis. Cells were then incubated with fresh medium for other 2 h and examined by confocal imaging. The co-localization ratio between Alexa647 and Lysotracker dropped from 69% to 31%, indicating the rapid lysosomal escape of DZ following DZ@ZIF-8 degradation (Figs. 5c and 5d).

We next investigated the intracellular cleavage of *CDR1as* by DZ@ZIF-8. Individual DZ1, DZ2, DZ3 or their combinations were used to construct DZ@ZIF-8 nanoparticles. These nanoparticles were then incubated with MCF-7 cells for 48 hours before quantifying *CDR1as* by RT-qPCR. The RNA levels of *CDR1as* decreased in all DZ@ZIF-8-treated cells. Particularly, the combination of DZ1+2 appeared to be the most efficient for *CDR1as* regulation (Fig. 5e), consistent with the result of transfected DZ (Fig. 3b). The combination of DZ1+2 was utilized for the synthesis of DZ@ZIF-8 complex in the subsequent experiment. The result indicated that DZ@ZIF-8 could downregulate *CDR1as* without the need of supplement of Zn^{2+}. Then, the mRNA levels of

downstream genes *RAF1* and *PIK3CD* were examined. DZ@ZIF-8 could downregulate the expression levels of both downstream genes to approximately 40% (Fig. 5f). To demonstrate the versatility of this DZ-based strategy for circRNA regulation, the nanocomplex containing 10-23 DNAzymes targeting the site1 and site2 on *CDR1as* was synthesized. Similarly, in the presence of Mg^{2+}, the 10DZ1+2@ZIF-8 complex could also downregulate the RNA levels of *CDR1as*, and those of downstream *RAF1* and *PIK3CD* (Figs. S5e and S5f).

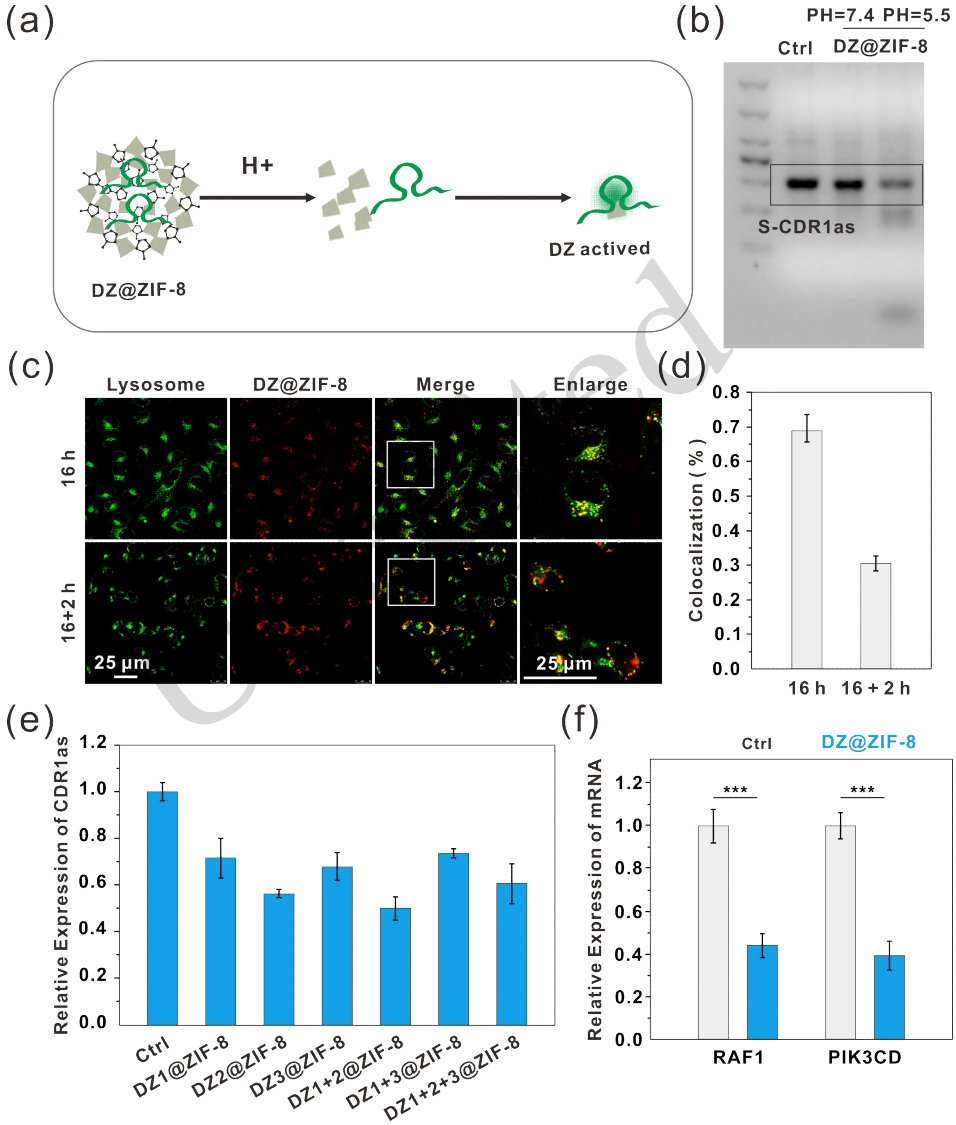

Fig. 5 Regulation of *CDR1as* and downstream genes by DZ@ZIF-8. (a) Schematic of acidic degradation of DZ@ZIF-8 and DZ activation. (b) Gel electrophoresis analysis of *CDR1as* cleavage under various pH conditions. (c) Lysosomal colocalization of Alexa647-DZ@ZIF-8 (30 μg/mL) was observed by confocal microscopy following a 16-hour incubation and LysoTracker Green staining (Lysosome: green; DZ@ZIF-8: red; Scale bar=25 μm). (d) Colocalization ratio of Alexa647-DZ@ZIF-8 with lysosomes quantified using ImageJ software (n20 cells). (e) mRNA levels of *CDR1as* upon treatment indicating DZ-loaded ZIF-8 determined by RT-qPCR. (f) RT-qPCR analysis of mRNA levels of RAF1 and PIK3CD treated with DZ@ZIF-8. Data are expressed as mean ± SD(n=3), *p < 0.05, **p < 0.01, ***p < 0.001. Abbreviations: ZIF-8, Zeolitic Imidazolate Framework-8; DZ, DNAzyme; mRNA, messenger RNA; *CDR1as, Cerebellar degeneration-related protein 1 antisense*.

2.4 Construction and application of dual functional DZ/MB@ZIF-8 in live cells

DZ@ZIF-8 could downregulate the RNA levels of *CDR1as*, liberating sequestered miR-7. This de-repression of miR-7 led to the inhibition of its downstream oncogenic targets (e.g., *RAF1*, *PIK3CD*). Therefore, by introducing a miR-7 targeting molecular beacon (MB), we could achieve simultaneous optical observation of the nanoplatform's activity (Fig. 6a). With the predictive assistance of MXfold2 software and RNAstructure software, a molecule beacon complementary to miR-7 was designed, with a fluorescent group Cy3 and a quenching group BHQ-2 modified at its two ends, respectively (Fig. S6a). Recognition and binding between miR-7 and this targeting MB was confirmed by gel electrophoresis (Fig. S6b). Next, the MB probe was incubated with miR-7 at gradually increasing concentrations from 0 to 200 nmol/L, and the fluorescence was measured. The results showed that the fluorescence intensity increased accordingly with the concentration of miR-7 (Fig. 6b).

Having validated the efficiency of MB for miR-7 detection, we constructed a dual functional ZIF-8-based nanocomplex co-encapsulating DZ and MB. Among them, DZ can cleave *CDR1as* and MB is responsible for evaluating the cleavage outcome by monitoring levels of miR-7. DZ/MB@ZIF-8 was synthesized and incubated with MCF-7 cells. The expression levels of the *CDR1as*/miR-7 axis were examined by RT-qPCR. Indeed, DZ/MB@ZIF-8 treatment downregulated *CDR1as* levels and caused an increase in miR-7 accordingly (Figs. 6c, 6d and S 6c). Notably, DZ/MB@ZIF-8 was more efficient to upregulate miR-7 than an equal amount of DZ that transfected via a transfection reagent and supplemented with Zn^{2+}, demonstrating the superiority of ZIF-8 to provide both effective DZ delivery and supply of essential Zn^{2+} co-factor.

To ensure that the fluorescence readout provides a quantitatively robust reflection of miR-7 levels without saturating the sensor, the nanoplatform was engineered to load molecular beacons (MBs) in a significant excess relative to the expected physiological miR-7 fluctuations. The reliability of this optical signal was further validated. Control experiments confirmed that the presence of the MB had not interfered with the reverse transcription or amplification efficiency of miR-7, and the robust fluorescence turn-on observed in live cells closely mirrored the miR-7 upregulation detected via RT-qPCR (Fig. S6c). Furthermore, the fluorescence properties of the Cy3 fluorophore remained highly stable across a pH range of 5.0 to 8.0 (Fig. S5d), eliminating the possibility of pH-induced artifacts during lysosomal degradation. Notably, while free DZ delivered by Lipofectamine 3000 (DZ/MB@lipo3000) could also cleave *CDR1as*, its efficiency was slightly lower than that achieved by DZ/MB@ZIF-8 (Fig. 6c).

Next, we explored DZ/MB@ZIF-8 for their capacity to monitor miR-7 in live cells. Upon treatment with DZ/MB@ZIF-8, obvious fluorescence signals could be observed. In contrast, cells treated with MB@ZIF-8 nanocomplex showed no fluorescence, demonstrating that DZ cleavage is necessary for miR-7 release (Fig. 6e). Concurrently, the results of flow cytometry analysis demonstrated a significant enhancement of intracellular fluorescence only in cells incubated with Complex DZ/MB@ZIF-8 (Fig. 6f). When a bifunctional nanocomplex

based on 10-23 DNAzyme (10DZ/MB@ZIF-8) was applied to MCF-7 cells in the presence of Mg^{2+}, both the downregulation of *CDR1as* RNA levels and increased fluorescence of miR-7 were observed (Fig. S6d and S6e).

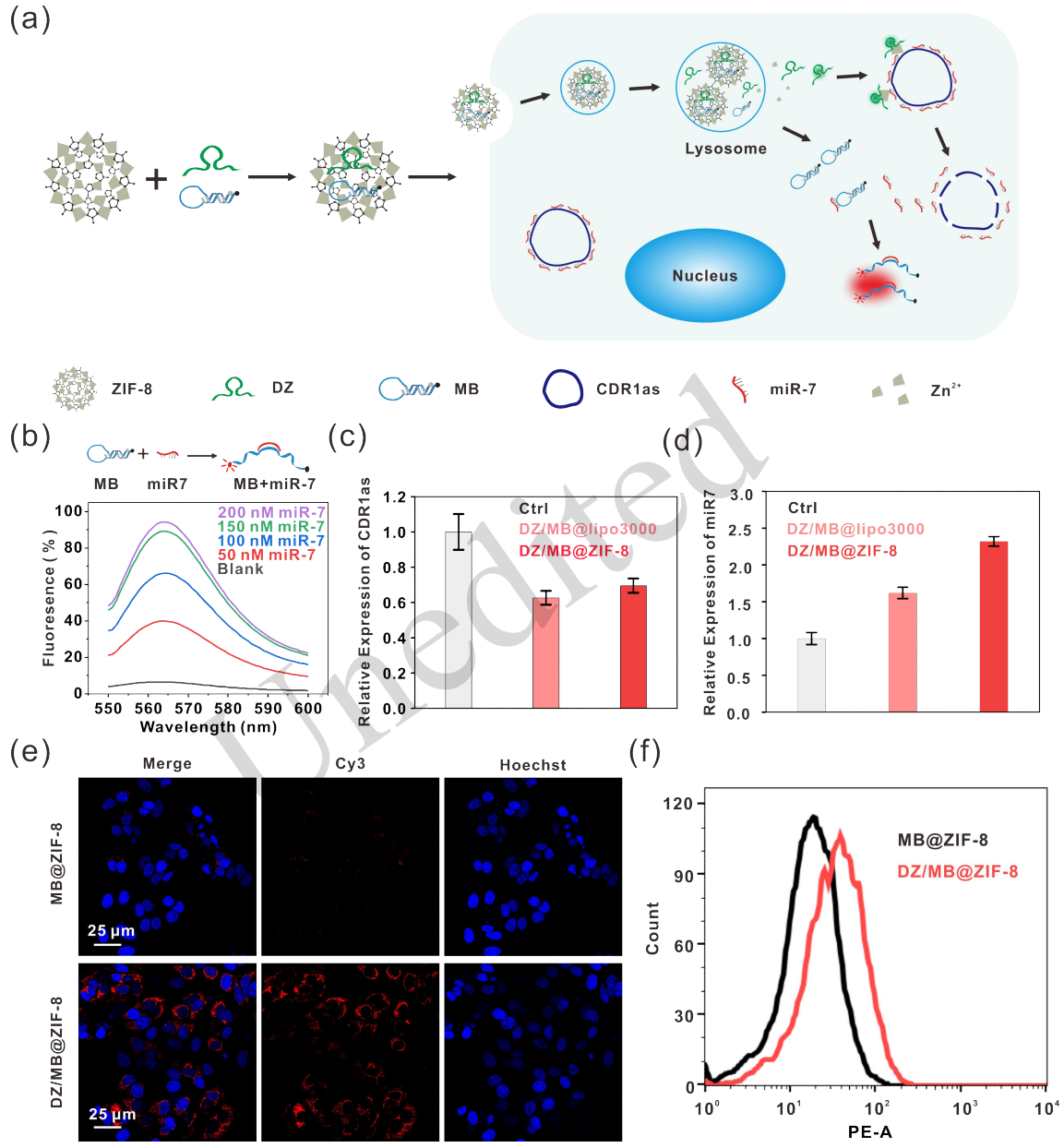

Fig. 6 Regulation and monitoring of the *CDR1as*/miR-7 axis by DZ/MB@ZIF-8. (a) Schematic diagram of intracellular process of DZ/MB@ZIF-8-mediated *CDR1as* cleavage and miR-7 sensing. (b) Fluorescence spectra of MB incubated with different concentrations of miR-7. (c) Levels of *CDR1as* treated with DZ/MB@ZIF-8 determined by RT-qPCR. (d) Levels of miR-7 treated with DZ/MB@ZIF-8 determined by RT-qPCR. (e) Confocal images of MCF-7 cells treated with MB@ZIF-8 or DZ/MB@ZIF-8. (Cy3: red; Hoechst: blue; Scale bar=25 μm). (f) Intracellular fluorescence intensity of MCF-7 cells treated with MB@ZIF-8 or DZ/MB@ZIF-8 measured by flow cytometry. All data are presented as mean ± SD from three independent biological replicates (n=3). Abbreviations: ZIF-8, Zeolitic Imidazolate Framework-8; DZ, DNAzyme; MB, molecular beacon; miR-7, microRNA-7; *CDR1as*, Cerebellar degeneration-related protein 1 antisense; lipo3000, Lipofectamine 3000.

Finally, the applicability of DZ/MB@ZIF-8 was investigated in cell lines other than MCF-7 cells. Human glioblastoma multiforme cells (U87 MG) and human embryonic kidney cells (HEK293T) were treated with DZ/MB@ZIF-8 and analyzed for *CDR1as* abundance and miR-7 imaging. DZ/MB@ZIF-8 could efficiently downregulate the RNA levels of *CDR1as* in both cells and showed increased fluorescence, as determined by flow cytometry analysis and confocal microscopy (Figs. 7a-7c, 7d-7e). The bifunctional nanocomplex 10DZ/MB@ZIF-8 was also applied to U87 MG cells and HEK293T cells in the presence of Mg^{2+}. The downregulation of *CDR1as* RNA levels and increased fluorescence of miR-7 were also observed (Figs. S7a-S7b, S7c-S7d). Therefore, the DNAzyme-based strategy for simultaneous *CDR1as* cleavage and miR-7 imaging exhibited excellent universality, adapting well to nanocomplexes constructed from various DNAzymes and proving applicable to multiple cell lines.

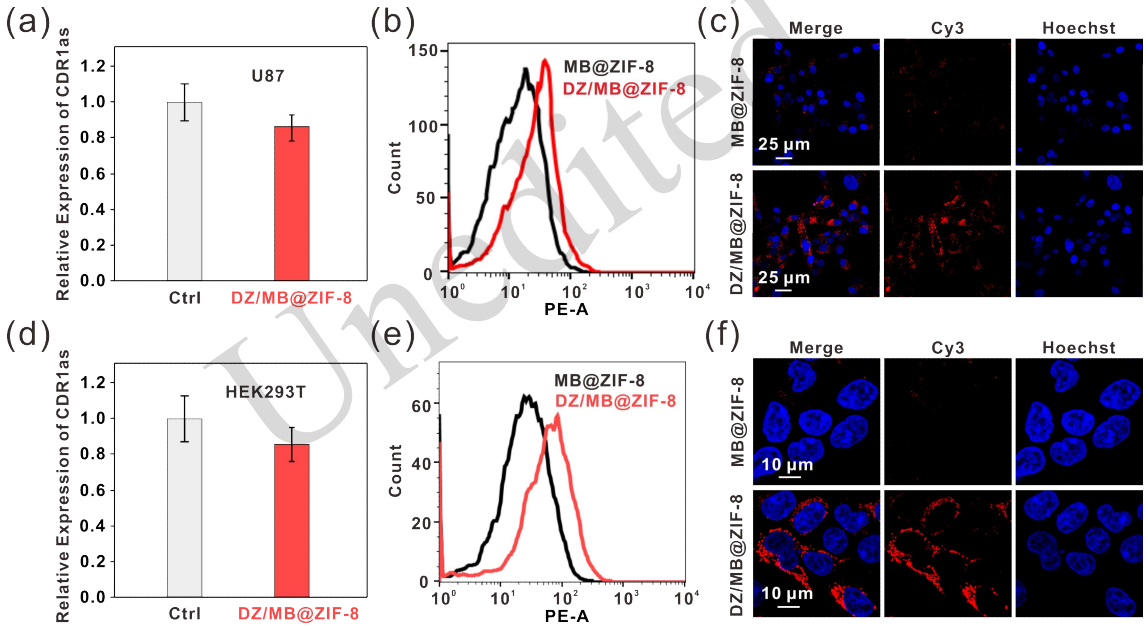

Fig. 7 Regulation and monitoring of the *CDR1as*/miR-7 axis in multiple cell lines by DZ/MB@ZIF-8. (a) mRNA levels of *CDR1as* in U87MG cells treated with DZ/MB@ZIF-8 determined by RT-qPCR. (b) Intracellular fluorescence intensity of U87MG cells treated with MB@ZIF-8 or DZ/MB@ZIF-8 measured by flow cytometry. (c) Confocal images of U87MG cells treated with MB@ZIF-8 or DZ/MB@ZIF-8. (Cy3: red; Hoechst: blue; Scale bar=25 μm). (d) mRNA levels of *CDR1as* in HEK293T cells treated with DZ/MB@ZIF-8 determined by RT-qPCR. (e) Intracellular fluorescence intensity of HEK293T cells treated with MB@ZIF-8 or DZ/MB@ZIF-8 measured by flow cytometry. (f) Confocal images of HEK293T cells treated with MB@ZIF-8 or DZ/MB@ZIF-8. (Cy3: red; Hoechst: blue; Scale bar=10 μm). All data are presented as mean±SD from three independent biological replicates (n=3). Abbreviations: ZIF-8, Zeolitic Imidazolate Framework-8; DZ, DNAzyme; MB, molecular beacon; miR-7, microRNA-7; mRNA, messenger RNA; *CDR1as*, *Cerebellar degenera-tion-related protein 1 antisense*.

3 Conclusions

In summary, we have developed a versatile theranostic nanoplatform, DZ/MB@ZIF-8, for the

simultaneous regulation and real-time monitoring of the oncogenic circRNA *CDR1as* and its downstream pathway. This system elegantly co-delivers a synergistic DNAzyme set for the efficient cleavage of *CDR1as* and a molecular beacon for miR-7 detection. The ZIF-8 carrier is not merely a passive vehicle; its pH-responsive degradation in lysosomes ensures triggered release of the functional agents while also supplying essential Zn^{2+} cofactors for optimal DNAzyme activity.

We have demonstrated that the targeted degradation of *CDR1as* de-represses miR-7, leading to the subsequent downregulation of key oncogenic targets, *RAF1* and *PIK3CD*. Crucially, this therapeutic effect is coupled with a direct, real-time fluorescent readout via the miR-7-sensing MB, enabling live-cell visualization of the platform's efficacy. The broad applicability of this approach was further validated across multiple cell lines and with alternative DNAzyme designs.

Overall, this work establishes a powerful strategy for the real-time functional analysis of circRNAs, moving beyond simple knockdown to integrated perturbation and validation. By providing a direct window into the dynamic circRNA-miRNA-mRNA regulatory network, our DZ/MB@ZIF-8 nanoplatform presents a promising tool for fundamental biological discovery and advances the development of circRNA-targeted cancer therapeutics.

Materials and methods

The materials and methods, Figs. S1-S7 and Table S1-S3 are provided in the electronic supplementary materials of this paper.

Data availability statement

The data that support the findings of this study are available from the corresponding author upon reasonable request.

Acknowledgments

This work is supported by the Natural Science Foundation of Shanghai (24ZR1455600), and National Natural Science Foundation of China (21974089).

Author contributions

Nan Chen conceived the study, coordinated the scientific team, wrote and edited the manuscript; Yan Huang, Jialin Ye and Lan Xu performed the experimental research and data analysis, wrote and edited the manuscript. Xingjie Hu contributed to the study design, data analysis, writing and editing of the manuscript. All authors read and approved the final manuscript and, therefore, had full access to all the data in the study and take responsibility for the integrity

and security of the data.

Compliance with ethics guidelines

The authors declare that they have no conflict of interest. This article does not contain any studies with human or animal subjects performed by any of the authors.

Declaration on the use of generative AI tools

No generative AI tools were used in the preparation of this manuscript.

References

Agarwal V, Bell GW, Nam J-W, et al., 2015. Predicting effective microrna target sites in mammalian mrnas. *eLife*, 4:e05005. https://doi.org/10.7554/eLife.05005

Ashwal-Fluss R, Meyer M, Pamudurti Nagarjuna r, et al., 2014. Circrna biogenesis competes with pre-mrna splicing. *Molecular Cell*, 56(1):55-66. https://doi.org/10.1016/j.molcel.2014.08.019

Behr M, Zhou J, Xu B, et al., 2021. In vivo delivery of crispr-cas9 therapeutics: Progress and challenges. *Acta Pharmaceutica Sinica B*, 11(8):2150-2171. https://doi.org/10.1016/j.apsb.2021.05.020

Bloomer H, Khirallah J, Li Y, et al., 2022. Crispr/cas9 ribonucleoprotein-mediated genome and epigenome editing in mammalian cells. *Advanced Drug Delivery Reviews*, 181:114087. https://doi.org/10.1016/j.addr.2021.114087

Breuer J, Barth P, Noe Y, et al., 2022. What goes around comes around: Artificial circular rnas bypass cellular antiviral responses. *Molecular Therapy - Nucleic Acids*, 28:623-635. https://doi.org/10.1016/j.omtn.2022.04.017

Cepeda-Plaza M, Peracchi A, 2020. Insights into DNA catalysis from structural and functional studies of the 8-17 dnazyme. *Organic & Biomolecular Chemistry*, 18(9):1697-1709. https://doi.org/10.1039/c9ob02453k

Chen H, Mao M, Jiang J, et al., 2019. Circular rna *CDR1as* acts as a sponge of mir-135b-5p to suppress ovarian cancer progression. *OncoTargets and Therapy*, Volume 12:3869-3879. https://doi.org/10.2147/ott.S207938

Chen K, Xu Y, Li J, et al., 2025. The potential and challenges of circular rna in the development of vaccines and drugs for emerging infectious diseases. *Molecular Therapy Nucleic Acids*, 36(3):102687. https://doi.org/10.1016/j.omtn.2025.102687

Fan S, Ma C, Tian X, et al., 2021. Detection of vibrio vulnificus in seafood with a dnazyme-based biosensor. *Frontiers in Microbiology*, 12:655845. https://doi.org/10.3389/fmicb.2021.655845

Feng C, Che X, Mao C, et al., 2025. Enhanced dnazyme-based tetrahedron amplifier for ultrasensitive determination and intracellular imaging of breast cancer-related micrornas. *ACS Sensors*, 10(11):8895-8905. https://doi.org/10.1021/acssensors.5c02856

Fuchs wightman F, Lukin J, Giusti Sebastián a, et al., 2024. Influence of rna circularity on target rna-directed microrna degradation. *Nucleic Acids Research*, 52(6):3358-3374. https://doi.org/10.1093/nar/gkae094

Gao W, Han X, Li L, et al., 2025. Functionalized zif-8 as a versatile platform for drug delivery and cancer therapy: Strategies, challenges and prospects. *Journal of Materials Chemistry B*, 13(12):3758-3785. https://doi.org/10.1039/d4tb02289k

Hansen TB, Jensen TI, Clausen BH, et al., 2013. Natural rna circles function as efficient microrna sponges. *Nature*, 495(7441):384-388. https://doi.org/10.1038/nature11993

Jeck WR, Sorrentino JA, Wang K, et al., 2013. Circular rnas are abundant, conserved, and associated with alu repeats. *Rna*, 19(2):141-157. https://doi.org/10.1261/rna.035667.112

Kihara AH, Ruda VM, Chandwani R, et al., 2014. The roles of individual mammalian argonautes in rna interference in vivo. *PLoS ONE*, 9(7):e101749. https://doi.org/10.1371/journal.pone.0101749

Lee M, Kang S, Kim S, et al., 2023. Advances and trends in mirna analysis using dnazyme-based biosensors. *Biosensors*, 13(9):856-875. https://doi.org/10.3390/bios13090856

Li C, Xu T, Hou G, et al., 2025. DNA nanotechnology-based strategies for gastric cancer diagnosis and therapy. *Materials Today Bio*, 30:101459. https://doi.org/10.1016/j.mtbio.2025.101459

Li R, Xu X, Gao S, et al., 2023. Circular rna *CDR1as* mediated by human antigen r (hur) promotes gastric cancer growth via mir-299-3p/tgif1 axis. *Cancers*, 15(23):5556-5576. https://doi.org/10.3390/cancers15235556

Liu C-X, Chen L-L, 2022. Circular rnas: Characterization, cellular roles, and applications. *Cell*, 185(12):2016-2034.

https://doi.org/10.1016/j.cell.2022.04.021
Liu Q-L, Zhang Z, Wei X, et al., 2021. Noncoding rnas in tumor metastasis: Molecular and clinical perspectives. *Cellular and Molecular Life Sciences*, 78(21-22):6823-6850. https://doi.org/10.1007/s00018-021-03929-0
Liu Q-W, He Y, Xu WW, 2022. Molecular functions and therapeutic applications of exosomal noncoding rnas in cancer. *Experimental & Molecular Medicine*, 54(3):216-225. https://doi.org/10.1038/s12276-022-00744-w
Liu R, Li J, Salena BJ, et al., 2024. Aptamer and dnazyme based colorimetric biosensors for pathogen detection. *Angewandte Chemie International Edition*, 64(4):e202418725. https://doi.org/10.1002/anie.202418725
Mao X, Cao Y, Guo Z, et al., 2021. Biological roles and therapeutic potential of circular rnas in osteoarthritis. *Molecular Therapy Nucleic Acids*, 24:856-867. https://doi.org/10.1016/j.omtn.2021.04.006
Mcconnell EM, Cozma I, Mou Q, et al., 2021. Biosensing with dnazymes. *Chemical Society Reviews*, 50(16):8954-8994. https://doi.org/10.1039/d1cs00240f
Mehta SL, Chokkalla AK, Bathula S, et al., 2023. *CDR1as* regulates α-synuclein-mediated ischemic brain damage by controlling mir-7 availability. *Molecular Therapy - Nucleic Acids*, 31:57-67. https://doi.org/10.1016/j.omtn.2022.11.022
Meng L, Ding P, Liu S, et al., 2020. The emerging prospects of circular rna in tumor immunity. *Annals of Translational Medicine*, 8(17):1091-1091. https://doi.org/10.21037/atm-19-4751
Mishra NO, Quon AS, Nguyen A, et al., 2023. Constructing physiological defense systems against infectious disease with metal–organic frameworks: A review. *ACS Applied Bio Materials*, 6(8):3052-3065. https://doi.org/10.1021/acsabm.3c00391
Nurmi C, Gu J, Mathai A, et al., 2024. Making target sites in large structured rnas accessible to rna-cleaving dnazymes through hybridization with synthetic DNA oligonucleotides. *Nucleic Acids Research*, 52(18):11177-11187. https://doi.org/10.1093/nar/gkae778
Odame E, Li L, Nabilla JA, et al., 2023. Mir-145-3p inhibits muscs proliferation and mitochondria mass via targeting mybl1 in jianzhou big-eared goats. *International Journal of Molecular Sciences*, 24(9):8341-8360. https://doi.org/10.3390/ijms24098341
Piwecka M, Glažar P, Hernandez-Miranda LR, et al., 2017. Loss of a mammalian circular rna locus causes mirna deregulation and affects brain function. *Science*, 357(6357):1254-1263. https://doi.org/10.1126/science.aam8526
Sato K, Akiyama M, Sakakibara Y, 2021. Rna secondary structure prediction using deep learning with thermodynamic integration. *Nature Communications*, 12(1):941-950. https://doi.org/10.1038/s41467-021-21194-4
Schubert S, 2003. Rna cleaving '10-23' dnazymes with enhanced stability and activity. *Nucleic Acids Research*, 31(20):5982-5992. https://doi.org/10.1093/nar/gkg791
Shafaghat Z, Radmehr S, Saharkhiz S, et al., 2025. Circular rna, a molecule with potential chemistry and applications in rna-based cancer therapeutics: An insight into recent advances. *Topics in Current Chemistry*, 383(2):21-56. https://doi.org/10.1007/s41061-025-00505-z
Shao Y, Xu J, Liang B, et al., 2023. The role of *CDR1as*/*ciRS-7* in cardio-cerebrovascular diseases. *Biomedicine & Pharmacotherapy*, 167:115589. https://doi.org/10.1016/j.biopha.2023.115589
Singh RR, Mondal I, Janjua T, et al., 2024. Engineered smart materials for rna based molecular therapy to treat glioblastoma. *Bioactive Materials*, 33:396-423. https://doi.org/10.1016/j.bioactmat.2023.11.007
Song G, Tian C, Li J, et al., 2023. Rapid characterization of anti-crispr proteins and optogenetically engineered variants using a versatile plasmid interference system. *Nucleic Acids Research*, 51(22):12381-12396. https://doi.org/10.1093/nar/gkad995
Troyano J, Carné-Sánchez A, Avci C, et al., 2019. Colloidal metal–organic framework particles: The pioneering case of zif-8. *Chemical Society Reviews*, 48(23):5534-5546. https://doi.org/10.1039/c9cs00472f
Victor J, Steger G, Riesner D, 2017. Inability of dnazymes to cleave rna in vivo is due to limited mg2+ concentration in cells. *European Biophysics Journal*, 47(4):333-343. https://doi.org/10.1007/s00249-017-1270-2
W S, Santoro, F.Joyce G, 1997. A general purpose rna-cleaving DNA enzyme. *Proc Natl Acad Sci USA*, 94 :4262–4266.
Wang H, Chen Y, Wang H, et al., 2019. Dnazyme‐loaded metal‐organic frameworks (mofs) for self‐sufficient gene therapy. *Angewandte Chemie International Edition*, 58(22):7380-7384. https://doi.org/10.1002/anie.201902714
Wang W, Sun L, Huang M-T, et al., 2023. Regulatory circular rnas in viral diseases: Applications in diagnosis and therapy. *RNA Biology*, 20(1):847-858. https://doi.org/10.1080/15476286.2023.2272118
Wei K, He M, Zhang J, et al., 2023. A DNA logic circuit equipped with a biological amplifier loaded into biomimetic

zif‐8 nanoparticles enables accurate identification of specific cancers in vivo. *Angewandte Chemie International Edition*, 62(41):e202307025. https://doi.org/10.1002/anie.202307025

Wu D, Liu X, Tang L, et al., 2024. Three-way junction-mediated three-letter coded sda cascade crispr/cas12a system for circrna detection. *Chemical Engineering Journal*, 497:154542. https://doi.org/10.1016/j.cej.2024.154542

Wu S, Zhang K, Liang Y, et al., 2021. Nano‐enabled tumor systematic energy exhaustion via zinc (ii) interference mediated glycolysis inhibition and specific glut1 depletion. *Advanced Science*, 9(7):2103534 https://doi.org/10.1002/advs.202103534

Xu B, Yang T, Wang Z, et al., 2018. Circrna *CDR1as*/mir-7 signals promote tumor growth of osteosarcoma with a potential therapeutic and diagnostic value. *Cancer Management and Research*, Volume 10:4871-4880. https://doi.org/10.2147/cmar.S178213

Xu C, Xu Y, Wang G, 2025. Bibliometric analysis of research on cervical cancer and mirnas from 2010 to 2024: Research trends, hotspots, and prospects. *Discover Oncology*, 16(1):1639-1654. https://doi.org/10.1007/s12672-025-03106-w

Yang J, Meng X, Pan J, et al., 2017. Crispr/cas9-mediated noncoding rna editing in human cancers. *RNA Biology*, 15(1):35-43. https://doi.org/10.1080/15476286.2017.1391443

Yang X, Ye T, Liu H, et al., 2021. Expression profiles, biological functions and clinical significance of circrnas in bladder cancer. *Molecular Cancer*, 20(1):4-29. https://doi.org/10.1186/s12943-020-01300-8

Ye J, Xie C, Wang C, et al., 2021. Promoting musculoskeletal system soft tissue regeneration by biomaterial-mediated modulation of macrophage polarization. *Bioactive Materials*, 6(11):4096-4109. https://doi.org/10.1016/j.bioactmat.2021.04.017

Yu H, Zhao Q, 2023. Dnazyme-based microscale thermophoresis sensor. *Analytical Chemistry*, 95(4):2152-2156. https://doi.org/10.1021/acs.analchem.2c04643

Zeng Z, Zhong M, Liao T, et al., 2024. Nano-fuels-driven self-sacrificed zif-8@apt integrated chip coupled with a dnazyme system for the isolation and detection of glioblastoma-derived extracellular vesicles. *Chemical Engineering Journal*, 502:157445. https://doi.org/10.1016/j.cej.2024.157445

Zhang X, Liu Q, Zhang T, et al., 2022. Bone-targeted nanoplatform enables efficient modulation of bone tumor microenvironment for prostate cancer bone metastasis treatment. *Drug Delivery*, 29(1):889-905. https://doi.org/10.1080/10717544.2022.2050845

Zhang Y, Huang X, Wang L, et al., 2021. Glutathionylation-dependent proteasomal degradation of wide-spectrum mutant p53 proteins by engineered zeolitic imidazolate framework-8. *Biomaterials*, 271 https://doi.org/10.1016/j.biomaterials.2021.120720

Zhang Y, Hu J, Qu X, et al., 2023. Circular rna rsu1 promotes retinal vascular dysfunction by regulating mir-345-3p/taz. *Communications Biology*, 6(1):719-731. https://doi.org/10.1038/s42003-023-05064-x

Zhao X, Cheng H, Wang Q, et al., 2023. Regulating photosensitizer metabolism with dnazyme-loaded nanoparticles for amplified mitochondria-targeting photodynamic immunotherapy. *ACS Nano*, 17(14):13746-13759. https://doi.org/10.1021/acsnano.3c03308

Zuker M, 2003. Mfold web server for nucleic acid folding and hybridization prediction. *Nucleic Acids Research*, 31(13):3406-3415. https://doi.org/10.1093/nar/gkg595